



Analyst

**Composition and Charge State Influence on the Ion-Neutral
Collision Cross Sections of Protonated N-Linked
Glycopeptides: An Experimental and Theoretical
Deconstruction of Coulombic Repulsion vs. Charge Solvation
Effects**

Journal:	<i>Analyst</i>
Manuscript ID	AN-ART-05-2019-000875.R1
Article Type:	Paper
Date Submitted by the Author:	10-Aug-2019
Complete List of Authors:	Gelb, Abby; University of Nebraska - Lincoln, Department of Chemistry Lai, Rui; University of Nebraska - Lincoln, Chemistry Li, Hui; University of Nebraska-Lincoln, Dodds, Eric; University of Nebraska - Lincoln, Department of Chemistry

SCHOLARONE™
Manuscripts

1
2
3
4
5
6
7
8
9
10

**COMPOSITION AND CHARGE STATE INFLUENCE ON THE
ION-NEUTRAL COLLISION CROSS SECTIONS OF PROTONATED N-LINKED GLYCOPEPTIDES:
AN EXPERIMENTAL AND THEORETICAL DECONSTRUCTION OF
COULOMBIC REPULSION VS. CHARGE SOLVATION EFFECTS**

11
12
13
14
15
16
17
18

Abby S. Gelb¹, Rui Lai¹, Hui Li^{1,2,3}, and Eric D. Dodds^{1,2*}

19
20
21

¹Department of Chemistry; ²Nebraska Center for Integrated Biomolecular Communication;

22
23

³Nebraska Center for Materials and Nanoscience

24
25

University of Nebraska – Lincoln

26
27
28

Lincoln, NE, 68588-0304, USA

29
30

*Corresponding Author

31
32

Department of Chemistry

33
34

University of Nebraska – Lincoln

35
36

711 Hamilton Hall, Lincoln, NE, 68588-0304, USA

37
38
39

E-mail: eric.dodds@unl.edu; Telephone: 1.402.472.3592

40
41
42

Submitted to *Analyst* for Consideration as a Full Paper

43
44

13 May 2019

45
46

Submitted in Revised Form

47
48
49

10 August 2019

50
51
52

KEYWORDS

53
54
55
56
57
58
59
60

Glycosylation; glycoproteins; glycopeptides; glycoproteomics; ion mobility spectrometry; ion-neutral collision cross section.

ABSTRACT

1
2
3
4
5 Ion mobility spectrometry (IMS) is of significant interest as a platform for glycoanalysis.
6
7 While much attention has been focused on the resolution of isomeric carbohydrates and
8
9 glycoconjugates, another appealing aspect of IMS is the ability to sort different classes of
10
11 biomolecules into distinct regions of mass vs. mobility space. This capability has potential to
12
13 greatly simplify glycoproteomic analyses, as glycosylated and non-glycosylated peptides can
14
15 be rapidly partitioned in the gas phase. Nevertheless, the physical and chemical
16
17 characteristics of glycopeptides that dictate their mass vs. mobility loci have yet to be
18
19 systematically investigated. This report presents an IMS study of model protonated
20
21 glycopeptide ions with systematically varied oligosaccharide topologies, polypeptide
22
23 sequences, and charge states. In all, over 110 ion-neutral collision cross sections (CCSs) were
24
25 measured and analyzed in the context of the physicochemical characteristics of the analytes.
26
27 Glycan size and composition emerged as a decisive factor in dictating the CCS space occupied
28
29 by the glycopeptides and exerted this influence in a charge state dependent fashion.
30
31 Furthermore, elongation of the glycan group was found to either increase or decrease
32
33 glycopeptide CCSs depending on the ion charge state and the size of the glycan. Molecular
34
35 dynamics (MD) simulations of the gas phase structures and CCSs of selected glycopeptides
36
37 revealed that the experimental observations were consistent with a glycan size and charge
38
39 state dependent interplay between destabilizing Coulombic repulsion effects (tending to result
40
41 in more extended structures) and stabilizing charge solvation effects in which the glycan plays
42
43 a major role (tending to result in more compact structures). Taken together, these IMS and
44
45 MD findings suggest the possibility of predicting and delineating glycopeptide-enriched
46
47 regions of mass vs. mobility space for applications in glycoproteomics.
48
49
50
51
52
53
54
55
56
57
58
59
60

INTRODUCTION

The combination of ion mobility spectrometry (IMS) with mass spectrometry (MS) to address needs in the field of glycoanalysis has gained considerable momentum in recent years.¹⁻⁴ Particularly vigorous study has been focused on pursuing the potential of IMS methods to rapidly resolve or distinguish isomeric carbohydrates in the gas phase.⁵⁻¹² Indeed, these efforts have resulted in significant progress towards alleviating the general isomer problem in oligosaccharide analysis. In a complementary fashion, IMS-MS methods also provide for the millisecond-order separation of different types of biomolecules into characteristic mass vs. mobility domains depending upon the intrinsic conformational ordering of various analyte classes.¹³⁻¹⁶ In the context of glycoproteomic analyses, accurate mass measurement^{17, 18} and tandem mass spectrometry (MS/MS) methods^{19, 20} are often used to infer site specific protein glycosylation profiles based on deduced compositions and structures of proteolytic glycopeptides.²¹⁻²⁶ In such experiments, the glycosylated complement of peptides is typically accompanied by a stoichiometrically more abundant ensemble of non-glycosylated peptides that tend to have more favorable ionization efficiencies than their glycan-bearing counterparts. The potential of IMS to achieve rapid partitioning of these ion populations presents an opportunity to enhance the selectivity and depth of glycoproteomic analyses. Encouragingly, the sorting of glycopeptides and peptides into unique mass vs. mobility coordinates was previously observed by Hill and coworkers when directly infusing an unfractionated tryptic digests of human- α_1 -acid glycoprotein and antithrombin III for IMS-MS analysis.²⁷ Aside from that study, surprisingly little else has been reported on glycopeptide analysis *via* IMS.²⁸⁻³³ In particular, the underlying compositional, structural, and physical determinants of glycopeptide mass vs. mobility sorting have not yet been scrutinized in detail. In this study, a collection of glycopeptides with systematically varied polypeptide sequences and oligosaccharide connectivities were prepared by tryptic proteolysis and exoglycosidase digestion. The resultant glycopeptides were analyzed by traveling wave ion mobility spectrometry (TWIMS) as protonated molecular ions in multiple charge states. TWIMS arrival

1
2
3 time distributions (ATDs) and ion-neutral collision cross sections (CCSs) were evaluated in
4 relation to the physicochemical features of the glycopeptides under study. Computational
5 chemistry methods were also applied to predict gas-phase structures for selected glycopeptide
6 ions and their corresponding CCSs. The combination of experimental and theoretical results
7 suggested some interesting glycan size dependent and charge state dependent relationships
8 between structure and CCS. These trends appeared to arise largely from transitions between
9 Coulombic repulsion controlled and charge solvation-controlled conformations, where in the
10 latter of these the glycan participated in stabilizing the sites of protonation. These results
11 imply that the domains of mass vs. mobility space that are occupied by glycopeptides can be
12 predicted from first principles and rationalized in terms of analyte characteristics. Collectively,
13 our findings also highlight the potential of an expanded role for IMS in glycoproteomic inquiry.
14
15
16
17
18
19
20
21
22
23
24
25
26

27 **EXPERIMENTAL**

28
29 ***N-Glycopeptide Preparation.*** RNase B from *Bos taurus* (UniProtKB P61823) was
30 acquired from Sigma-Aldrich (St. Louis, MO, USA). Model glycopeptides were generated by
31 tryptic digestion of the target glycoprotein as previously described elsewhere.³⁴⁻³⁸ Briefly, a
32 50 μL aliquot of RNase B stock solution (2 $\mu\text{g}/\mu\text{L}$ in 8 M urea and 50 mM ammonium
33 bicarbonate, pH 7.5) was mixed with 10 μL of 450 mM dithiothreitol and incubated for 1 h at
34 55°C to reduce disulfide linkages. The resulting free thiols were acetamidated by addition of
35 10 μL of 500 mM iodoacetamide, followed by a 1 h incubation in the dark and at room
36 temperature. The mixture was next combined with 175 μL of 50 mM ammonium bicarbonate
37 (pH 7.5) and 5 μL of 0.5 $\mu\text{g}/\mu\text{L}$ proteomics grade trypsin (Sigma-Aldrich), then incubated for
38 18 h at 37°C. Tryptic digests prepared in this manner were either subjected to N-glycan
39 truncation or directly purified and analyzed with the glycans intact.
40
41
42
43
44
45
46
47
48
49
50

51 ***N-Glycan Truncation.*** Glycopeptides harboring smaller N-glycan structures were
52 prepared *via* sequential exoglycosidase digestion of the tryptic peptides using $\alpha(1\rightarrow2,3)$ and
53
54
55
56
57
58
59
60

1
2
3 $\alpha(1\rightarrow6)$ mannosidases (New England Biolabs; Ipswich, MA, USA). Initially, 2 μL of 0.1 nmol/ μL
4
5 $\alpha(1\rightarrow2,3)$ mannosidase was added to the glycopeptide preparation, followed by incubation at
6
7 37°C. The digestion was allowed to proceed for a total of 18 h, with a subsample of the digest
8
9 being taken after 2 h incubation. The 18 h digest was then subsampled prior to treatment
10
11 with 2 μL of 0.1 nmol/ μL $\alpha(1\rightarrow6)$ mannosidase. Incubation was again carried out at 37°C,
12
13 with samples again being taken following 2 h and 18 h digestion. The resulting preparations
14
15 were subsequently purified and analyzed as detailed below.

16
17
18 ***N-Glycopeptide Purification.*** N-glycopeptides were purified according to previously
19
20 described protocols.³⁴⁻³⁸ In short, each digest of interest was vacuum centrifuged using a
21
22 Speed Vac SC110 (Thermo Savant, Holbrook, NY, USA) to reduce the volume from 150-250
23
24 μL to approximately 10 μL . The digests were reconstituted to approximately 100 μL by
25
26 addition of 0.1% formic acid. Glycopeptide desalting and enrichment was then performed
27
28 using solid phase extraction (SPE) micropipette tips loaded with zwitterionic hydrophilic
29
30 interaction liquid chromatography (ZIC-HILIC) stationary phase (Protea Biosciences;
31
32 Somerset, NJ, USA). The ZIC-HILIC SPE tip was first wet with water, equilibrated with 80%
33
34 acetonitrile / 0.1% formic acid, then loaded with a 20 μL portion of reconstituted digest. The
35
36 tip was next washed with 80% acetonitrile / 0.1% formic acid and eluted into 20 μL of 0.1%
37
38 formic acid.

39
40 ***Ion Mobility Spectrometry and Mass Spectrometry.*** All IMS and MS
41
42 measurements were carried out using a Synapt G2-S HDMS TWIMS-MS instrument (Waters,
43
44 Manchester, UK) equipped with a modified static-mode nanoflow electrospray ionization (nESI)
45
46 source. Glass nESI emitters were fashioned from Pyrex melting point capillaries (100 mm x
47
48 1.5-1.8 mm; Corning, NY, USA) using a vertical micropipette puller (David Kopf Instruments,
49
50 Tujunga, CA, USA). The nESI emitters were loaded with 10 μL of analyte solution and fitted
51
52 onto the ion source stage using an electrode holder (Warner Instruments, Holliston, MA, USA)
53
54 such that a platinum wire (Alfa Aesar, Haverhill, MA, USA) applied the nESI capillary potential
55
56
57
58
59
60

1
2
3 directly to the analyte solution. The nESI capillary potential was optimized for each emitter
4 and was typically in the range 1.0-1.5 kV. The sampling cone voltage was adjusted between
5
6 10–20 V, the source offset voltage was set to 10 V, and the source temperature was held at
7
8 80°C. During TWIMS analysis, the helium cell gas flow was set to 180 mL/min, with the flow
9
10 of nitrogen to the mobility cell set to 60 mL/min. The trap DC bias was held constant at 44 V,
11
12 the TWIMS traveling DC wave height was held constant at 40 V, and the TWIMS traveling DC
13
14 wave velocity was held constant at 650 m/s. The RF amplitudes applied to the stacked ring
15
16 ion guides in the pre-TWIMS, TWIMS, and post-TWIMS regions of the instrument were 350 V
17
18 (trap cell), 250 V (TWIMS cell), and 380 V (transfer cell). Initial data analysis and processing
19
20 was carried out in MassLynx 4.1 and DriftScope 2.7 (Waters). Further data analysis and
21
22 visualization was accomplished using SigmaPlot 13 (Systat, Chicago, IL, USA) and with
23
24 custom routines written and implemented in IGOR Pro 7 (WaveMetrics, Lake Oswego, OR,
25
26 USA).

27
28
29 ***Ion-Neutral Collision Cross Section Calibration.*** Drift times measured by TWIMS
30
31 were converted to CCS values using previously described calibration procedures.^{8, 9, 39-42} To
32
33 concisely summarize, protonated polyalanine ions were used as CCS calibrants since these
34
35 are among the most well-characterized and broadly adopted calibrants for CCS measurement
36
37 by TWIMS.⁴³⁻⁵⁰ Advantageously, both He and N₂ CCSs have been established for these ion
38
39 series, allowing their use as standards for the measurement of analyte CCSs on either a He
40
41 or N₂ basis.⁴⁴ Although CCSs are more commonly reported for He drift gas, N₂ CCS values are
42
43 likely to be more relevant to TWIMS experiments carried out using N₂ drift gas. Therefore,
44
45 both values are reported in this work. The polyalanine mixture (Sigma-Aldrich) was prepared
46
47 at 12.5 µg/µL in 50% acetonitrile / 0.1% formic acid and analyzed as described above.
48
49 Calibration curves were then generated that related the known He and N₂ CCSs of the
50
51 polyalanine peptides to their corresponding TWIMS drift times. Separate calibration curves
52
53 were constructed for each drift gas (He and N₂), and for each ion charge state considered (z
54
55 = +2 and z = +3). The CCSs of doubly charged and triply charged analytes were measured
56
57
58
59
60

1
2
3 using the corresponding charge state matched calibration as previously recommended.⁴²
4
5 While every effort was made to ensure the reliability of this widely accepted calibration
6
7 method, we acknowledge that some non-idealities may arise from calibrating TWIMS drift
8
9 times to CCSs in this manner. However, prior work suggests that this procedure results in
10
11 CCS errors that are comparable to the inherent reproducibility of these measurements.⁴²
12

13 **Computational Chemistry.** Gas phase structures and CCSs were computed using a
14
15 previously reported method.⁵¹ Briefly, global minimum structures of glycopeptide ions were
16
17 identified by using the Merck Molecular Force Field force field (MMFF94)⁵²⁻⁵⁵ and a simple
18
19 molecular dynamics (MD) optimization method implemented in the Quantum Chemistry
20
21 Polarizable Force Field program (QuanPol)⁵⁶ which is integrated in the General Atomic and
22
23 Molecular Electronic Structure System (GAMESS).^{57, 58} In this optimization approach (QuanPol
24
25 keyword MDOPT=1000), an MD simulation is conducted at 600 K. Every 1000 MD steps, the
26
27 MD is paused, but not interrupted, for a steepest descent geometry optimization to locate a
28
29 minimum-energy structure. The globally optimized ion structures were then used for MD
30
31 simulations (100 ns each) of the ion mobility in He or N₂ drift gases. Force field parameters
32
33 for He and N₂ drift gases are described in **Tables S1-S2** of the **Electronic Supplementary**
34
35 **Information**. In all the simulations, 512 He atoms or N₂ molecules were included in a cubic
36
37 periodic boundary condition (PBC) box with fixed side length of 77.04 Å for He and 131.74 Å
38
39 for N₂. The volumes of the ions, estimated by using a density of 1.0 g/cm³, were deducted
40
41 from the total volume. The MD simulations were performed with drift gases at 290 K. The
42
43 average pressure was ~50 bar for He, and ~10 bar for N₂. The electric fields were selected
44
45 so that they resulted in Townsend numbers (~30–40 Td) and drift velocities (~200 m/s and
46
47 ~80 m/s in He and N₂, respectively) that were comparable to experimental conditions. As a
48
49 result, the effective thermodynamic ion temperatures (considering vibrations and rotations)
50
51 were all controlled at 300 ± 2 K. The average temperature of the ions (without considering
52
53 ion drift) were also around 300 K.
54
55
56
57
58
59
60

1
2
3 A mixed force field was used for the ion and gas system. The partial atomic charges,
4 bond stretching terms, bond angle bending terms, stretching-bending coupling terms,
5 dihedral rotation terms and wagging terms for the ion atoms were from the original MMFF94
6 force field. Conventional 12-6 Lennard-Jones (LJ) terms were used for interactions between
7 the ion atoms (note the original MMFF94 uses a drifted 14-7 LJ), between the gas atoms, and
8 between the ion atoms and gas atoms. The 12-6 LJ potential parameters for the ion atoms
9 are shown in **Tables S1-S2** of the **Electronic Supplementary Information**. Within the ion,
10 the LJ potentials were excluded for the 1-2 and 1-3 atom pairs that were described with bond
11 stretching and bending terms and were fully included for the 1-4 atoms. Due to the use of a
12 PBC, a switching function was used for the LJ potential (QuanPol keywords ISWITCH=2,
13 SWRA=10.0 Å, SWRB=12.0 Å).

14
15 The dipole polarization of the He and N₂ molecules were included by using the dipole
16 polarizability from experiments (0.2051 Å³ for He; 1.740 Å³ for N₂; see **Tables S1-S2** of the
17 **Electronic Supplementary Information**).^{59, 60} No polarizability points were used for the ion
18 atoms. The QuanPol keyword IDOPOL=1 was used so the mutual polarization between the
19 gas molecules was not considered. This is identical to the R^{-4} charge-polarizability potential
20 commonly used in trajectory methods. Due to the use of a PBC, a switching function was used
21 for the charge-polarizability potential (QuanPol keywords IPOLSHF=0, ISWITCH=2,
22 SWRA=10.0 Å, SWRB=12.0 Å).

23 24 25 **RESULTS**

26
27 **Overview.** The model glycoprotein RNase B was selected to provide tryptic N-
28 glycopeptide ions with multiple amino acid sequences (NLTK, SRNLTK, NLTKDR, SRNLTKDR),
29 glycan compositions (GlcNAc₂ + Man_{*n*}, or simply "Man *n*," with *n* = 1-8), and charge states
30 (doubly and triply protonated) appropriate for a study of physical and chemical factors
31 affecting the glycopeptide CCSs. Over the course of this study, some interesting trends in
32 measured CCS were noted that prompted the consideration of N-glycopeptides with truncated
33
34
35
36
37
38
39
40
41
42
43
44
45
46
47
48
49
50
51
52
53
54
55
56
57
58
59
60

1
2
3 glycans in addition to the intact, native N-glycans (Man5 through Man8). Thus, a sequential
4 exoglycosidase digestion strategy was used to produce the Man1 through Man4 glycopeptides,
5 as illustrated in **Figure 1**. In all, over 110 CCS values were obtained for this pool of analytes.
6
7 Computational modeling and prediction of theoretical CCSs were also performed to rationalize
8 several key experimental findings in structural and conformational terms.
9
10

11
12
13 **Glycopeptide Arrival Time Distributions.** The TWIMS ATDs for all doubly and triply
14 protonated glycoforms of SRNLTK, NLTKDR, and SRNLTKDR are presented in **Figure 2**. As
15 expected, the doubly and triply charged glycopeptides sort into distinct drift time windows
16 (2.5–5.0 ms for $z = 2+$; 1.5–3.0 ms for $z = 3+$). Interestingly, very different shifts in ATD
17 position were observed with the addition of each mannose residue. In general, the doubly
18 protonated ions exhibited more uniform shifts between successive glycoforms, with the
19 inclusion of additional mannose residues shifting the ATDs to longer drift times in comparable
20 increments. Some exceptions to this trend can be found, perhaps most notably in the very
21 small shift in drift time observed between the doubly protonated Man4 and Man5 glycoforms
22 of SRNLTK (**Figure 2a**). Nevertheless, the addition of monosaccharide units tended to shift
23 the mobilities of the doubly charged glycopeptides in a monotonic and incremental fashion.
24 By contrast, the triply charged glycopeptides demonstrated markedly different behavior
25 characterized by highly variable shifts in mobility with successive addition of monosaccharides.
26 Indeed, in several cases involving the triply protonated glycoforms of SRNLTK and NLTKDR,
27 the order of arrival time did not follow the size of the glycan (**Figures 2b, 2d**). In both of
28 these instances, the ATDs for Man3–Man6 glycoforms were heavily overlapped, with larger
29 gaps in drift time separating the lower and higher glycoforms. The triply protonated
30 SRNLTKDR glycopeptides exhibited some compression of the ATDs for the intermediate
31 glycoforms; however, the order of arrival times still followed the mannose number of the
32 glycan involved. Overall, these findings were interpreted as potentially revealing of an
33 interplay between Coulombic repulsion effects (which tend to bring about more extended gas
34 phase structures to minimize charge-charge interactions) and charge solvation effects (which
35
36
37
38
39
40
41
42
43
44
45
46
47
48
49
50
51
52
53
54
55
56
57
58
59
60

1
2
3 could result in more compact structures owing to increased intramolecular interaction
4 contributing to stabilization of charge sites). The dependence on glycan size also suggested
5 some involvement of the glycan moiety in charge solvation, at least for sufficiently large
6 glykans.
7
8
9
10

11 **Glycopeptide Collision Cross Sections.** In **Figure 3**, all measured He and N₂ CCSs
12 values are visualized as a function of m/z , which resulted in distinct groupings of the doubly
13 and triply charged glycopeptide ions. The CCS values and their uncertainties are provided in
14 **Table S3** of the **Electronic Supplementary Information**. Regardless of whether the CCS
15 values were calibrated to a He or N₂ axis, the doubly protonated glycopeptide ions under
16 study generally exhibited a rather linear increase in CCS as a function of m/z . The only
17 contribution to increasing m/z for a given peptide group was the addition of mannose residues,
18 resulting in the Man1–Man8 glycoforms. Thus, increases in CCS increased in direct proportion
19 to the number of mannose residues for the doubly charged ions under investigation. This
20 result is consistent with a previous finding of Costello and coworkers, which demonstrated
21 linear increases in the CCSs of various glycopeptides as monosaccharide residues were
22 added.³² Contrastingly, the triply charged glycopeptide ions examined here exhibited
23 significantly greater scatter in the CCS dimension, particularly in the region about 600 m/z .
24 Interestingly, CCSs of the Man1–Man8 glycoforms of the triply charged SRNLTKDR peptide
25 increased in an approximately linear fashion, similar to the behavior noted for the doubly
26 charged glycopeptides. This may be related to the larger size of the peptide group and the
27 presence of an additional stably protonated amino acid side chain. Overall, these results are
28 consistent with the observations noted from the TWIMS ATDs and demonstrate that
29 glycopeptide ion mobilities can scale with glycan size in charge state dependent manners that
30 may seem counterintuitive upon initial examination.
31
32
33
34
35
36
37
38
39
40
41
42
43
44
45
46
47
48
49
50

51 **Trends in Charge State and Glycan Size Dependence.** CCS values for the $z = 2+$
52 and $z = 3+$ ions from each glycoform of SRNLTK, NLTKDR, and SRNLTKDR are directly
53 compared in **Figure 4**. Overall, the $z = 3+$ glycopeptide ions were consistently found to have
54
55
56
57
58
59
60

1
2
3 significantly larger CCS values than their $z = 2+$ counterparts for the smaller glycoforms
4 studied (Man1–Man4); however, the larger glycoforms (Man5–Man8) exhibited more varied
5 behavior with respect to the relative CCSs of the doubly and triply charged ions. For instance,
6 He CCSs for the SRNLTK glycoforms (**Figure 4a**) were significantly larger for $z = 3+$ ions
7 between Man1 and Man4, but for Man5–Man8 the $z = 2+$ CCSs were found to be larger.
8 Comparable trends can be seen for the He CCSs of NLTKDR and SRNLTKDR glycoforms, as
9 well (**Figures 4c,e**). When viewed as N_2 CCSs, this reversal in relative size was not apparent
10 for any of the peptide compositions involved; however, in some cases the gap in N_2 CCS
11 between the $z = 2+$ and $z = 3+$ forms of the glycopeptides was found depend heavily on the
12 glycoform at hand. For SRNLTK and NLTKDR, this gap was initially quite large for the Man1
13 species but had diminished significantly by the Man8 glycoform (**Figure 4b,d**). A similar,
14 though less pronounced manifestation of this behavior was also noted for the N_2 CCSs of the
15 SRNLTKDR glycoforms (**Figure 4f**). In aggregate, these comparisons suggest that Coulombic
16 repulsion is a major driving force dictating the conformations of the smaller glycoforms,
17 forcing these triply charged ions into extended structures that are markedly larger than those
18 of their doubly charged counterparts. Meanwhile, for the larger glycoforms, the CCS
19 differences between $z = 2+$ and $z = 3+$ ions are far less pronounced, suggesting that the
20 addition of mannose residues allows the doubly and triply charged ions to take on similar
21 CCSs. This is intriguing, since the addition of neutral monosaccharide residues would not seem
22 to provide favorable new sites of protonation to a glycopeptide ion already containing multiple
23 sites of high gas phase basicity. Thus, the means by which the triply protonated structures
24 achieve CCSs similar to the corresponding doubly protonated form may not be through the
25 relief of charge-charge interaction by accessing alternative protonation motifs during the nESI
26 process. Instead, there is also the possibility that intramolecular interactions, perhaps driven
27 by charge solvation and involving the glycan itself, lead to the generation of more compact
28 structures. Furthermore, the ability to sample these condensed conformers may depend on
29 the glycan being of sufficient size to facilitate the decisive interactions.
30
31
32
33
34
35
36
37
38
39
40
41
42
43
44
45
46
47
48
49
50
51
52
53
54
55
56
57
58
59
60

1
2
3
4 **Structural Corollaries from Computational Modeling.** Global minimization of
5 doubly charged glycopeptides SRNLTK with N-glycan compositions and structures of
6 GlcNAc₂Man₁₋₆ indicated that, when the peptides are protonated at the arginine residue and
7 the N-terminal serine (the C-terminal lysine is not protonated), the ions have lower energies,
8 as seen in **Figure 5** and all models shown in **Figure S1** of the **Electronic Supplementary**
9 **Information**. The simulated He and N₂ CCS values for these doubly and triply charged
10 glycopeptides are shown in **Table S4** of the **Electronic Supplementary Information**. In
11 general, the triply charged glycopeptides have larger simulated CCS values than the
12 corresponding doubly charged ions. This is mainly caused by the higher charge state, but
13 conformational differences also contribute significantly. As shown in **Figure 4**, the doubly
14 charged ions are more compact than their triply charged counterparts. With the addition of a
15 third proton on the C-terminal lysine residue and thus stronger internal Coulomb repulsion,
16 triply charged glycopeptides tend to be less compact and exhibit larger CCS values. However,
17 as the glycan becomes larger (*e.g.*, Man5 and Man6), the internal Coulomb repulsion becomes
18 less severe, so the compactness of triply charged glycopeptides is comparable to the doubly
19 charged counterparts. Another contributing factor may be the size dependence of charge-gas
20 interaction: larger sized ions tend to exhibit weaker electric fields due to greater charge
21 delocalization, so their charge induced dipole interactions are lower. The glycopeptides with
22 larger oligosaccharide structures also have more atoms that can provide stronger internal
23 self-solvation of the charges *via* intramolecular hydrogen bonding and charge-dipole
24 interaction. The net effect of these contributions was that, doubly and triply charged
25 glycopeptide ions with larger glycans (*e.g.*, Man5 and Man6) tend to have more similar CCSs
26 than those with smaller glycans (*e.g.*, Man1-3). For example, in N₂ gas, the difference
27 between simulated CCS values of doubly and triply charged SRNLTK + GlcNAc₂Man₅ is 26 Å²,
28 and the CCS difference between doubly and triply charged SRNLTK + GlcNAc₂Man₆ is 23 Å².
29 These differences are significantly smaller than those for SRNLTK + GlcNAc₂Man₁ (48 Å²
30 difference between $z = +2$ and $z = +3$), SRNLTK + GlcNAc₂Man₂ (57 Å² difference between z
31
32
33
34
35
36
37
38
39
40
41
42
43
44
45
46
47
48
49
50
51
52
53
54
55
56
57
58
59
60

1
2
3 = +2 and $z = +3$), and SRNLTK + GlcNAc₂Man₃ (67 Å² difference between $z = +2$ and $z =$
4 +3). The simulated results are in good agreement with the experimental data, as the average
5 percent difference between experimental and theoretical CCSs was 3.8% for He CCSs and
6 2.3% for N₂ CCSs (see **Table S4** of the **Electronic Supplementary Information**). Full
7 Cartesian coordinates for all modeled glycopeptide ions are provided in **Table S5** of the
8 **Electronic Supplementary Information**.

17 **CONCLUSIONS**

19 For the glycopeptides studied here, some general conclusions can be drawn regarding
20 the influence of charge state and glycan size upon the mobility of their doubly and triply
21 protonated ions. As size of the glycan is increased from Man1 to Man8, the TWIMS arrival
22 times and CCSs of both doubly and triply charged ions generally tend to increase.
23 Nevertheless, there also appear to be pivotal transition regions for some triply charged ions
24 in which the addition of monosaccharide units causes the ion mobilities, as monitored through
25 ATDs and CCSs, to plateau or even decrease before eventually increasing again. We note here
26 that similar qualitative trends have been well-documented in IMS analyses of synthetic
27 polymers.⁶¹⁻⁶⁵ Distinct grouping of $z = 2+$ and $z = 3+$ ions was observed in CCS vs. m/z space,
28 though the manner in which the various glycoforms of each peptide were distributed depended
29 to a large extent on the charge state. Direct comparisons of CCSs for the doubly and triply
30 protonated series of peptide glycoforms suggests an interplay between two competing modes
31 of structural stabilization: minimizing Coulombic repulsion and maximizing charge solvation.
32 The CCS dependencies observed appear to suggest that the glycan moiety itself participates
33 in charge stabilizing intermolecular interactions, though this is only possible for glycans of
34 sufficient size to participate in these interactions. When the glycan has been truncated such
35 that these interactions are no longer accessible, Coulombic repulsion is the major driver of
36 the glycopeptide ion conformation. These structural arguments were supported by MD
37 simulations of the gas phase ion structures and MD based CCS prediction. The latter of these
38
39
40
41
42
43
44
45
46
47
48
49
50
51
52
53
54
55
56
57
58
59
60

1
2
3 produced N₂ CCS values that agreed with experimental results to within 2.3%, on average.
4
5 On the whole, these results provide useful fundamental insights into some physical and
6
7 structural determinants of glycopeptide ion sorting in IMS. Such insights have potential to
8
9 facilitate the further development of IMS as an analytical tool for glycoproteomic analysis.
10

11 12 13 **ACKNOWLEDGEMENTS**

14
15 Funding from the National Institutes of Health, National Institute of General Medical
16
17 Sciences, supported this work through a Maximizing Investigators' Research Award to E.D.D.
18
19 (grant number R35GM128926), a fellowship to A.S.G. from the Molecular Mechanisms of
20
21 Disease Predoctoral Training Program (grant number T32GM107001), and a seed grant to H.L.
22
23 and E.D.D from the Nebraska Center for Integrated Biomolecular Communication (grant
24
25 number P20GM113126). Funding to E.D.D. from the National Science Foundation, Division of
26
27 Chemistry, through the Chemical Measurement and Imaging Program (grant number 1507989)
28
29 is also acknowledged. This work was carried out using core facilities supported in part by the
30
31 National Institutes of Health, National Institute of General Medical Sciences through the
32
33 Nebraska Center for Integrated Biomolecular Communication (grant number P20GM113126).
34
35 Computational chemistry calculations were performed using resources at the University of
36
37 Nebraska Holland Computing Center. Finally, A.S.G. would like to thank Dr. Yuting Huang for
38
39 valued guidance and mentorship in the early stages of this project.
40
41
42
43

44 **ELECTRONIC SUPPLEMENTARY INFORMATION**

45
46 Electronic supplementary information (ESI) is available: Tabulated atomic charges,
47
48 Lennard-Jones potentials, and dipole polarizabilities used in the molecular dynamics
49
50 simulations of ion mobility; tabulated experimental ion-neutral collision cross section values;
51
52 tabulated comparisons of experimental and theoretical ion-neutral collision cross section
53
54 values; gas-phase structures for additional selected glycopeptide ions; and Cartesian
55
56 coordinates of optimized gas-phase glycopeptide structures.
57
58
59
60

1
2
3
4
5
6
7
8
9
10
11
12
13
14
15
16
17
18
19
20
21
22
23
24
25
26
27
28
29
30
31
32
33
34
35
36
37
38
39
40
41
42
43
44
45
46
47
48
49
50
51
52
53
54
55
56
57
58
59
60

AUTHOR ORCID IDENTIFIERS

Abby S. Gelb: 0000-0003-3752-4898

Eric D. Dodds: 0000-0002-7721-394X

REFERENCES

1. Y. Huang, A. S. Gelb and E. D. Dodds, *Curr. Metabolom.*, 2013, **1**, 291-305.
2. C. J. Gray, B. Thomas, R. Upton, L. G. Migas, C. E. Evers, P. E. Barran and S. L. Flitsch, *Biochim. Biophys. Acta*, 2016, **1860**, 1688-1709.
3. J. Hofmann and K. Pagel, *Angew. Chem.*, 2017, **56**, 8342-8349.
4. K. A. Morrison and B. H. Clowers, *Curr. Opin. Chem. Biol.*, 2018, **42**, 119-129.
5. B. H. Clowers, P. Dwivedi, W. E. Steiner, H. H. Hill Jr and B. Bendiak, *J. Am. Soc. Mass Spectrom.*, 2005, **16**, 660-669.
6. J. P. Williams, M. Grabenauer, R. J. Holland, C. J. Carpenter, M. R. Wormald, K. Giles, D. J. Harvey, R. H. Bateman, J. H. Scrivens and M. T. Bowers, *Int. J. Mass Spectrom.*, 2010, **298**, 119-127.
7. L. S. Fenn and J. A. McLean, *Phys. Chem. Chem. Phys.*, 2011, **13**, 2196-2205.
8. Y. Huang and E. D. Dodds, *Anal. Chem.*, 2013, **85**, 9728-9735.
9. Y. Huang and E. D. Dodds, *Analyst*, 2015, **140**, 6912-6921.
10. Y. Huang and E. D. Dodds, *Anal. Chem.*, 2015, **87**, 5664-5668.
11. J. Hofmann, H. S. Hahm, P. H. Seeberger and K. Pagel, *Nature*, 2015, **526**, 241-244.
12. X. Zheng, X. Zhang, N. S. Schocker, R. S. Renslow, D. J. Orton, J. Khamsi, R. A. Ashmus, I. C. Almeida, K. Tang, C. E. Costello, R. D. Smith, K. Michael and E. S. Baker, *Anal. Bioanal. Chem.*, 2017, **409**, 467-476.
13. L. S. Fenn and J. A. McLean, *Anal. Bioanal. Chem.*, 2008, **391**, 905-909.
14. L. S. Fenn, M. Kliman, A. Mahsut, S. R. Zhao and J. A. McLean, *Anal. Bioanal. Chem.*, 2009, **394**, 235-244.
15. J. A. McLean, *J. Am. Soc. Mass Spectrom.*, 2009, **20**, 1775-1781.
16. J. C. May, C. R. Goodwin, N. M. Lareau, K. L. Leaptrot, C. B. Morris, R. T. Kurulugama, A. Mordehai, C. Klein, W. Barry and E. Darland, *Anal. Chem.*, 2014, **86**, 2107-2116.
17. H. Desaire and D. Hua, *Int. J. Mass Spectrom.*, 2009, **287**, 21-26.

- 1
- 2
- 3 18. J. W. Froehlich, E. D. Dodds, M. Wilhelm, O. Serang, J. A. Steen and R. S. Lee, *Mol.*
- 4 *Cell. Proteomics*, 2013, **12**, 1017-1025.
- 5
- 6
- 7 19. M. Wuhrer, M. I. Catalina, A. M. Deelder and C. H. Hokke, *J. Chromatogr. B*, 2007,
- 8 **849**, 115-128.
- 9
- 10
- 11 20. E. D. Dodds, *Mass Spectrom. Rev.*, 2012, **31**, 666-682.
- 12
- 13 21. D. S. Dalpathado and H. Desaire, *Analyst*, 2008, **133**, 731-738.
- 14
- 15 22. H. J. An, J. W. Froehlich and C. B. Lebrilla, *Curr. Opin. Chem. Biol.*, 2009, **13**, 421-
- 16 426.
- 17
- 18
- 19 23. W. R. Alley, Jr., B. F. Mann and M. V. Novotny, *Chem. Rev.*, 2013, **113**, 2668-2732.
- 20
- 21 24. H. Desaire, *Mol. Cell. Proteomics*, 2013, **12**, 893-901.
- 22
- 23 25. V. Kolli, K. N. Schumacher and E. D. Dodds, *Bioanalysis*, 2015, **7**, 113-131.
- 24
- 25 26. S. Gaunitz, G. Nagy, N. L. B. Pohl and M. V. Novotny, *Anal. Chem.*, 2017, **89**, 389-
- 26 413.
- 27
- 28
- 29 27. H. Li, B. Bendiak, W. F. Siems, D. R. Gang and H. H. Hill, *Int. J. Ion Mobil. Spectrom.*,
- 30 2013, **16**, 105-115.
- 31
- 32
- 33 28. A. J. Creese and H. J. Cooper, *Anal. Chem.*, 2012, **84**, 2597-2601.
- 34
- 35 29. P. Both, A. P. Green, C. J. Gray, R. Sardzik, J. Voglmeir, C. Fontana, M. Austeri, M.
- 36 Rejzek, D. Richardson and R. A. Field, *Nat. Chem.*, 2014, **6**, 65.
- 37
- 38
- 39 30. H. Hinneburg, J. Hofmann, W. B. Struwe, A. Thader, F. Altmann, D. Varón Silva, P. H.
- 40 Seeberger, K. Pagel and D. Kolarich, *Chem. Commun.*, 2016, **52**, 4381-4384.
- 41
- 42 31. J. L. Campbell, T. Baba, C. Liu, C. S. Lane, J. C. Y. Le Blanc and J. W. Hager, *J. Am.*
- 43 *Soc. Mass Spectrom.*, 2017, **28**, 1374-1381.
- 44
- 45 32. R. S. Glaskin, K. Khatri, Q. Wang, J. Zaia and C. E. Costello, *Anal. Chem.*, 2017, **89**,
- 46 4452-4460.
- 47
- 48
- 49
- 50
- 51 33. A. Barroso, E. Giménez, A. Konijnenberg, J. Sancho, V. Sanz-Nebot and F. Sobott, *J.*
- 52 *Proteomics*, 2018, **173**, 22-31.
- 53
- 54
- 55 34. V. Kolli and E. D. Dodds, *Analyst*, 2014, **139**, 2144-2153.
- 56
- 57
- 58
- 59
- 60

- 1
2
3 35. F. Aboufazeli, V. Kolli and E. D. Dodds, *J. Am. Soc. Mass Spectrom.*, 2015, **26**, 587-
4 595.
5
6
7 36. V. Kolli, H. A. Roth, G. De La Cruz, G. S. Fernando and E. D. Dodds, *Anal. Chim. Acta*,
8 2015, **896**, 85-92.
9
10
11 37. V. Kolli, K. N. Schumacher and E. D. Dodds, *Analyst*, 2017, **142**, 4691-4702.
12
13 38. F. Aboufazeli and E. D. Dodds, *Analyst*, 2018, **143**, 4459-4468.
14
15 39. B. T. Ruotolo, J. L. P. Benesch, A. M. Sandercock, S. J. Hyung and C. V. Robinson, *Nat.*
16 *Protoc.*, 2008, **3**, 1139-1152.
17
18
19 40. K. Thalassinou, M. Grabenauer, S. E. Slade, G. R. Hilton, M. T. Bowers and J. H.
20 Scrivens, *Anal. Chem.*, 2008, **81**, 248-254.
21
22
23 41. D. Smith, T. Knapman, I. Campuzano, R. Malham, J. Berryman, S. Radford and A.
24 Ashcroft, *Eur. J. Mass Spectrom.*, 2009, **15**, 113-130.
25
26
27 42. A. S. Gelb, R. E. Jarratt, Y. Huang and E. D. Dodds, *Anal. Chem.*, 2014, **86**, 11396-
28 11402.
29
30
31 43. S. C. Henderson, J. Li, A. E. Countermand and D. E. Clemmer, *J. Phys. Chem. B*, 1999,
32 **103**, 8780-8785.
33
34
35 44. M. F. Bush, I. D. G. Campuzano and C. V. Robinson, *Anal. Chem.*, 2012, **84**, 7124-
36 7130.
37
38
39 45. I. Campuzano, M. F. Bush, C. V. Robinson, C. Beaumont, K. Richardson, H. Kim and
40 H. I. Kim, *Anal. Chem.*, 2012, **84**, 1026-1033.
41
42
43 46. K. Pagel and D. J. Harvey, *Anal. Chem.*, 2013, **85**, 5138-5145.
44
45
46 47. J. Hofmann, W. B. Struwe, C. A. Scarff, J. H. Scrivens, D. J. Harvey and K. Pagel, *Anal.*
47 *Chem.*, 2014, **86**, 10789-10795.
48
49
50 48. G. Paglia, J. P. Williams, L. Menikarachchi, J. W. Thompson, R. Tyldesley-Worster, S.
51 Halldorsson, O. Rolfsson, A. Moseley, D. Grant, J. Langridge, B. O. Palsson and G.
52 Astarita, *Anal. Chem.*, 2014, **86**, 3985-3993.
53
54
55
56
57
58
59
60

- 1
- 2
- 3
- 4 49. J. G. Forsythe, A. S. Petrov, C. A. Walker, S. J. Allen, J. S. Pellissier, M. F. Bush, N. V.
- 5 Hud and F. M. Fernandez, *Analyst*, 2015, **140**, 6853-6861.
- 6
- 7 50. K. M. Hines, J. C. May, J. A. McLean and L. Xu, *Anal. Chem.*, 2016, **88**, 7329-7336.
- 8
- 9 51. R. Lai, E. D. Dodds and H. Li, *J. Chem. Phys.*, 2018, **148**, 064109.
- 10
- 11 52. T. A. Halgren, *J. Comput. Chem.*, 1996, **17**, 520-552.
- 12
- 13 53. T. A. Halgren, *J. Comput. Chem.*, 1996, **17**, 553-586.
- 14
- 15 54. T. A. Halgren and R. B. Nachbar, *J. Comput. Chem.*, 1996, **17**, 587-615.
- 16
- 17 55. T. A. Halgren, *J. Comput. Chem.*, 1996, **17**, 616-641.
- 18
- 19 56. N. M. Thellamurege, D. J. Si, F. C. Cui, H. B. Zhu, R. Lai and H. Li, *J. Comput. Chem.*,
- 20 2013, **34**, 2816-2833.
- 21
- 22
- 23 57. M. W. Schmidt, K. K. Baldrige, J. A. Boatz, S. T. Elbert, M. S. Gordon, J. H. Jensen,
- 24 S. Koseki, N. Matsunaga, K. A. Nguyen, S. J. Su, T. L. Windus, M. Dupuis and J. A.
- 25 Montgomery, *J. Comput. Chem.*, 1993, **14**, 1347-1363.
- 26
- 27 58. M. S. Gordon and M. W. Schmidt, in *Theory and Applications of Computational*
- 28 *Chemistry*, eds. C. E. Dykstra, G. Frenking, K. S. Kim and G. E. Scuseria, Elsevier,
- 29 Amsterdam, 2005, DOI: <https://doi.org/10.1016/B978-044451719-7/50084-6>, pp.
- 30 1167-1189.
- 31
- 32
- 33
- 34
- 35
- 36
- 37 59. A. C. Newell and R. C. Baird, *J. Appl. Phys.*, 1965, **36**, 3751-3759.
- 38
- 39 60. G. R. Alms, A. K. Burnham and W. H. Flygare, *J. Chem. Phys.*, 1975, **63**, 3321-3326.
- 40
- 41 61. S. Trimpin and D. E. Clemmer, *Anal. Chem.*, 2008, **80**, 9073-9083.
- 42
- 43 62. S. M. Weidner and S. Trimpin, *Anal. Chem.*, 2010, **82**, 4811-4829.
- 44
- 45 63. D. Morsa, T. Defize, D. Dehareng, C. Jerome and E. De Pauw, *Anal. Chem.*, 2014, **86**,
- 46 9693-9700.
- 47
- 48
- 49 64. J. R. N. Haler, J. Far, A. Aqil, J. Claereboudt, N. Tomczyk, K. Giles, C. Jerome and E.
- 50 De Pauw, *J. Am. Soc. Mass Spectrom.*, 2017, **28**, 2492-2499.
- 51
- 52 65. C. Wesdemiotis, *Angew. Chem. Int. Ed.*, 2017, **56**, 1452-1464.
- 53
- 54
- 55
- 56
- 57
- 58
- 59
- 60

FIGURE CAPTIONS

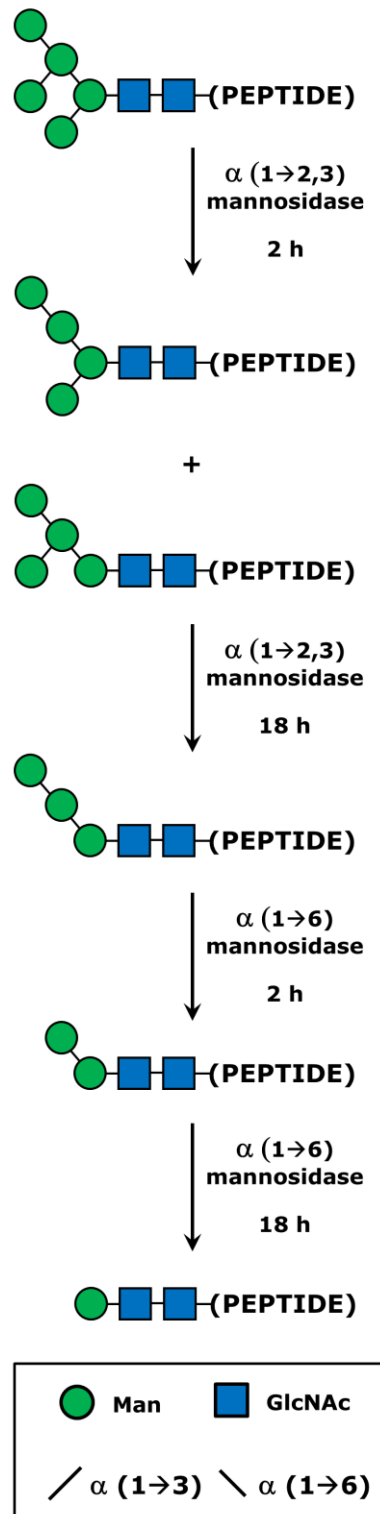
Figure 1. Schematic summary of the enzymatic deconstruction of N-glycan moieties to yield truncated N-glycopeptides. For simplicity, this process is illustrated starting with the smallest and most abundant RNase B glycoform, Man5. The larger N-glycans present in the mixture would be decomposed in a similar fashion. Glycopeptide preparations were first treated with $\alpha(1\rightarrow2,3)$ mannosidase, which after a 2 h yielded a mixture of Man4 structures *via* hydrolysis of one of the two susceptible glycosidic linkages of Man5. With 18 h of incubation, both $\alpha(1\rightarrow3)$ linked residues were cleaved from Man5, producing the Man3 structure. The digest was next treated with $\alpha(1\rightarrow6)$ mannosidase, which sequentially degraded the remaining branch of Man3 to yield Man2 and Man1 after 2 h and 18 h of incubation, respectively. A key to the monosaccharide and glycosidic bond symbology is provided in the inset.

Figure 2. Representative TWIMS ATDs for the Man1 through Man8 glycoforms of SRNLTK with $z = 2+$ (**a**) and $z = 3+$ (**b**); NLTKDR with $z = 2+$ (**c**) and $z = 3+$ (**d**); and SRNLTKDR with $z = 2+$ (**e**) and $z = 3+$ (**f**). Each ATD is labelled with the number of mannose residues comprising the corresponding glycoform.

Figure 3. CCS (Ω) vs. mass-to-charge ratio (m/z) for all glycopeptides measured, with TWIMS arrival times calibrated to provide He (**a**) and N₂ (**b**) CCS values. Where visible, error bars represent the standard deviation of four replicate measurements.

1
2
3 **Figure 4.** CCS (Ω) for the Man1 through Man8 glycoforms of SRNLTk as doubly protonated
4 and triply protonated ions calibrated to He (**a**) and N₂ (**b**) drift gases; the Man1
5 through Man8 glycoforms of NLTkDR as doubly protonated and triply protonated ions
6 calibrated to He (**c**) and N₂ (**d**) drift gases; and the Man1 through Man8 glycoforms
7 of SRNLTkDR as doubly protonated and triply protonated ions calibrated to He (**e**) and
8 N₂ (**f**) drift gases. For each glycoform, the CCS values measured for the $z = 2+$ charge
9 state (solid bars) are compared to those for the $z = 3+$ charge state (hatched bars).
10 Where visible, error bars represent the standard deviation of four replicate
11 measurements.
12
13
14
15
16
17
18
19
20
21
22

23 **Figure 5.** Energy-minimized gas phase structures of the SRNLTk + GlcNAc₂Man₁ glycopeptide
24 with $z = 2+$ (**a**) and $z = 3+$ (**b**); and the SRNLTk + GlcNAc₂Man₅ glycopeptide with z
25 = $2+$ (**c**) and $z = 3+$ (**d**). The corresponding experimentally measured (Ω_{expt}) and
26 theoretically calculated (Ω_{calc}) N₂ CCS values are indicated for each ion.
27
28
29
30
31
32
33
34
35
36
37
38
39
40
41
42
43
44
45
46
47
48
49
50
51
52
53
54
55
56
57
58
59
60

FIGURES**Figure 1.**

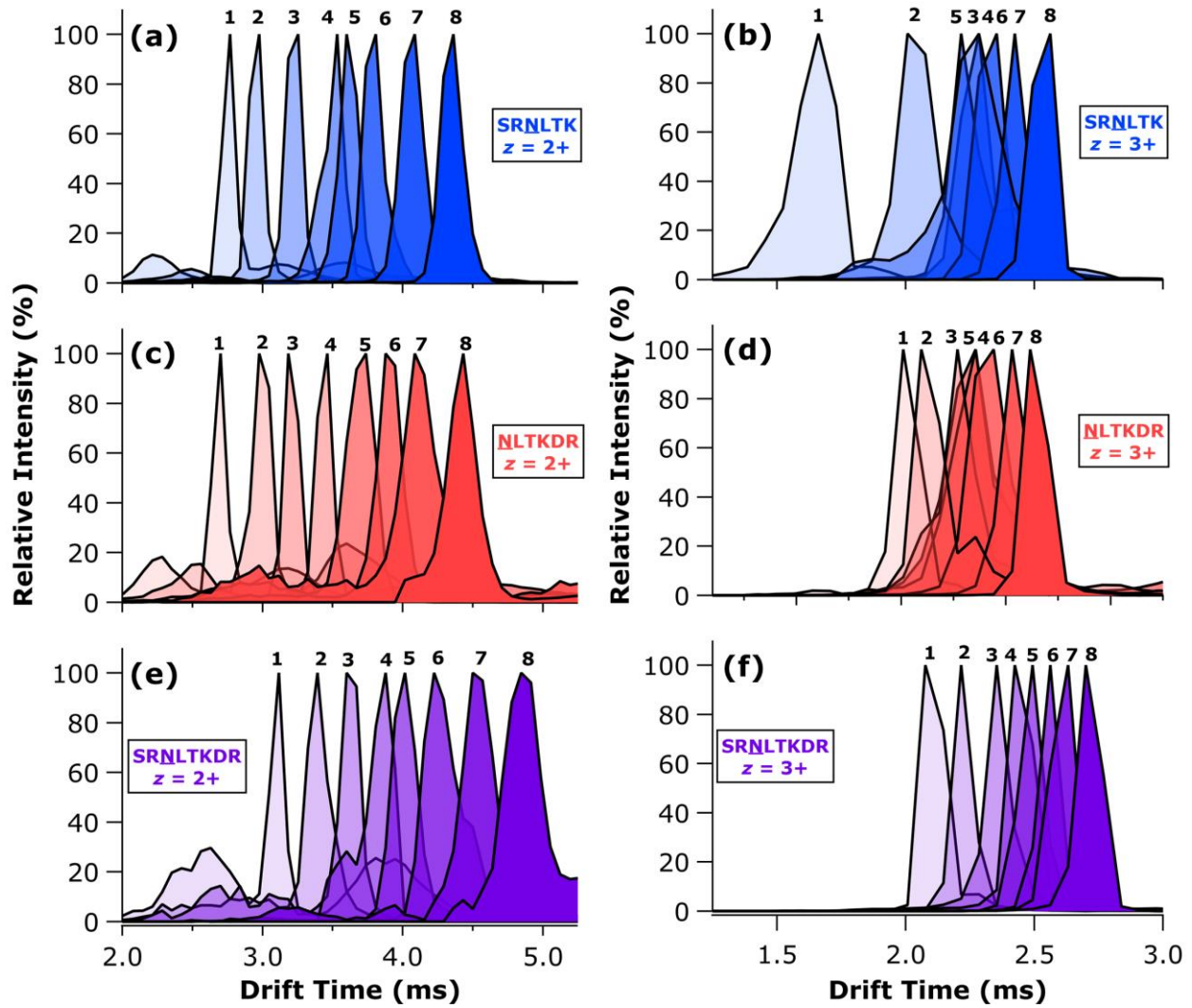
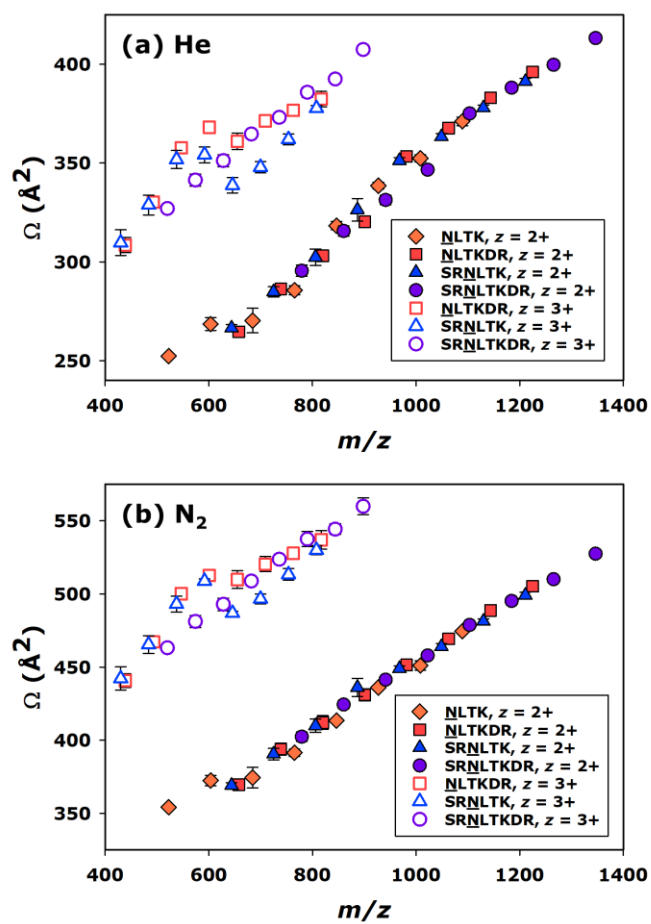


Figure 2.

**Figure 3.**

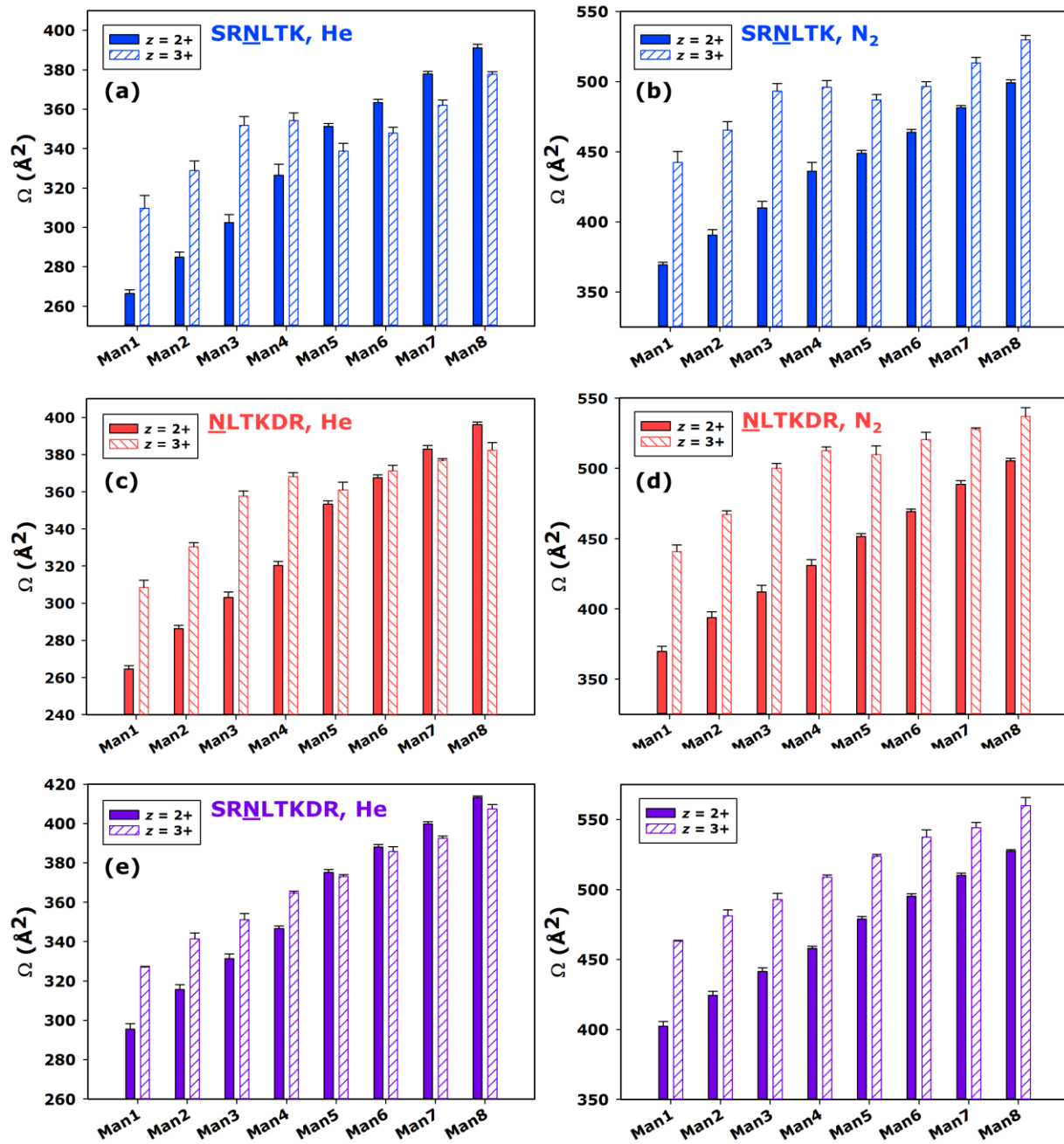


Figure 4.

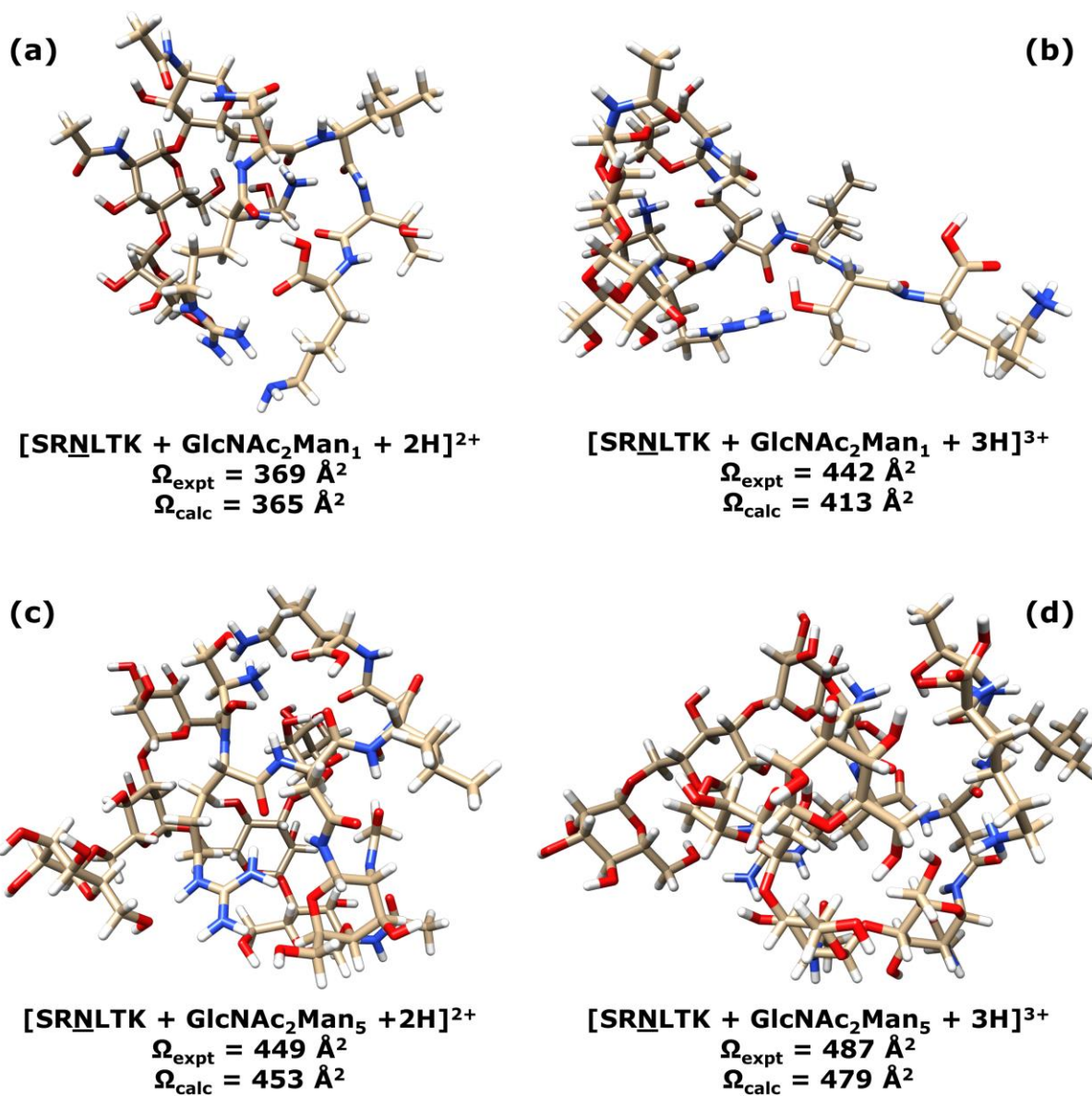
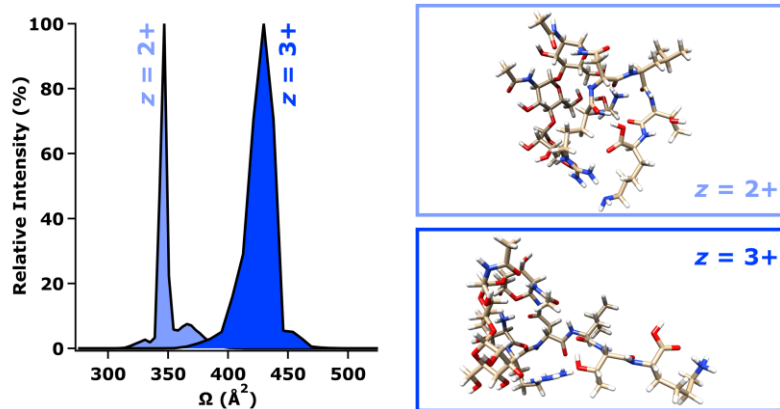


Figure 5.

GRAPHICAL ABSTRACT**TEXTUAL ABSTRACT**

This study suggests the possibility of predicting and delineating glycopeptide-enriched regions of mass vs. mobility space for applications in glycoproteomics.